Amine–Borane Dehydropolymerization

International Edition: DOI: 10.1002/anie.201600898
German Edition: DOI: 10.1002/ange.201600898

The Simplest Amino-borane $H_2B{=}NH_2$ Trapped on a Rhodium Dimer: Pre-Catalysts for Amine–Borane Dehydropolymerization

Amit Kumar, Nicholas A. Beattie, Sebastian D. Pike, Stuart A. Macgregor, and Andrew S. Weller**

Abstract: *The μ-amino–borane complexes $[Rh_2(L^R)_2(\mu\text{-}H)(\mu\text{-}H_2B{=}NHR')][BAr^F{}_4]$ ($L^R{=}R_2P(CH_2)_3PR_2$; $R = Ph$, ^iPr; $R' = H$, Me) form by addition of $H_3B{\cdot}NMeR'H_2$ to $[Rh(L^R)(\eta^6\text{-}C_6H_5F)][BAr^F{}_4]$. DFT calculations demonstrate that the amino–borane interacts with the Rh centers through strong Rh-H and Rh-B interactions. Mechanistic investigations show that these dimers can form by a boronium-mediated route, and are pre-catalysts for amine-borane dehydropolymerization, suggesting a possible role for bimetallic motifs in catalysis.*

Polyamino-boranes ($[H_2BNRH]_n$) are potentially exciting new materials that are isoelectronic with technologically pervasive polyolefins, but are chemically distinct because of (δ−)HB−NH(δ+) polarization. They are formed by the dehydropolymerization of amine-boranes ($H_3B{\cdot}NRH_2$; R = H or Me, for example; Scheme 1 A),[1] and metal-catalyzed routes to polyamino-boranes offer the potential for fine control over molecular weight and polymer stereochemistry.

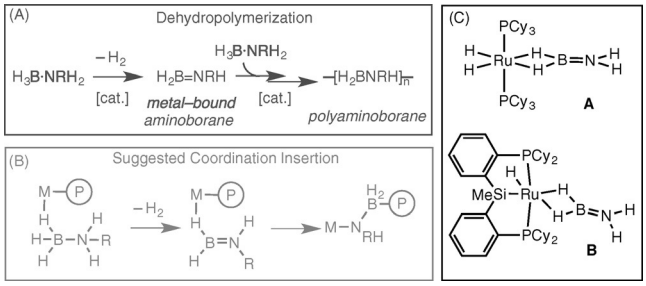

Scheme 1. A) Amine-borane dehydropolymerization; B) a suggested coordination/insertion mechanism, P = polymer chain; C) examples of $H_2B{=}NH_2$ coordinated to a metal center.

[*] A. Kumar, Dr. S. D. Pike, Prof. A. S. Weller
Department of Chemistry, Chemistry Research Laboratories, University of Oxford, Mansfield Road, Oxford, OX1 3TA (UK)
E-mail: andrew.weller@chem.ox.ac.uk
N. A. Beattie, Prof. S. A. Macgregor
Institute of Chemical Sciences, Heriot Watt University, Edinburgh, EH14 4AS (UK)
E-mail: S.A.Macgregor@hw.ac.uk

Supporting information for this article can be found under: http://dx.doi.org/10.1002/anie.201600898.

There is recent evidence that these processes occur at a metal center in which the catalyst needs to perform two roles: 1) formal dehydrogenation of amine-borane to form a latent source of amino-borane ($H_2B{=}NRH$), and 2) subsequent B−N bond formation.[2–6] For some systems a coordination/insertion mechanism is proposed, although the precise structure of the propagating species is currently unresolved (Scheme 1 B).[3,5,6] This is in contrast to olefin polymerization, in which the feedstock (for example, ethene or propene) is already unsaturated, and the active species and propagating mechanisms are well-defined.[7] A clearer understanding of how the catalyst dehydrogenates amine-borane, traps intermediate amino-boranes, and promotes B−N bond-formation, is central to harnessing the full potential of systems that ultimately deliver new well–defined B−N polymeric materials on a useful scale.

Unlike ethene ($H_2C{=}CH_2$), which is stable under ambient conditions, the isoelectronic amino-borane ($H_2B{=}NH_2$) has only been prepared in low temperature matrices and oligomerizes above −150 °C.[2,8] Adding steric bulk to the nitrogen atom increases stability, so that, for example, $H_2B{=}NMeH$[9] or $H_2B{=}N^tBuH$[10] can be observed as transient species using in situ NMR spectroscopy before they also oligomerize. There are two examples where unstable $H_2B{=}NH_2$ can be trapped by coordination to a single metal center. These originate after dehydrogenation of a putative σ-ammonia borane[11] complex, forming $Ru(PCy_3)_2(H)_2(\eta^2\text{-}H_2B{=}NH_2)$ **A**[12] and (Cy-PSiP)-$Ru(H)(\eta^2\text{-}H_2B{=}NH_2)$ **B**, Cy-PSiP = κ^3-$(Cy_2PC_6H_4)_2SiMe$).[13]

We now report that $H_2B{=}NH_2$ can be trapped by a bimetallic $[Rh_2(R_2PCH_2CH_2CH_2PR_2)_2]^{2+}$ fragment to give a novel bridging amino-borane bonding motif. We provide mechanistic evidence for formation of the complex from a monometallic precursor, and show that such dimeric amino-borane species may be important in dehydropolymerization pathways. This report builds upon previous observations that indirectly implicate bimetallic motifs during catalysis.[14–16]

Addition of a slight excess of $H_3B{\cdot}NH_3$ to a $[D_8]$THF solution of $[Rh(L^{Ph})(\eta^6\text{-}C_6H_5F)][BAr^F{}_4]$ **1** ($L^{Ph} = Ph_2P(CH_2)_3PPh_2$, $Ar^F = 3,5\text{-}(CF_3)_2C_6H_3$) resulted in the rapid formation of a bimetallic monocation, which was identified by NMR spectroscopy, electrospray ionization mass spectrometry (ESI-MS), and single-crystal X-ray diffraction, as $[Rh_2(L^{Ph})_2(\mu\text{-}H)(\mu\text{-}H_2B{=}NH_2)][BAr^F{}_4]$ **3**. One equivalent of the boronium[9,17–20] cation $[THF{\cdot}BH_2{\cdot}NH_3][BAr^F{}_4]$ was also formed ($\delta(^{11}B)$ 0.5 (t), $J_{BH} = 108$ Hz; lit.[19] $[Et_2O{\cdot}BH_2{\cdot}NH_3][BAr^F{}_4]$ $\delta(^{11}B)$ 0.2, $J_{BH} = 125$ Hz).

In situ solution NMR data for **3** show a signal at $\delta(^{11}B)$ 51.5, a single ^{31}P environment ($\delta(^{31}P)$ 18.2, $J_{RhP} = 142$ Hz), and a broad peak at $\delta(^1H)$ −7.45 (integral ca. 3H relative to the

phenyl groups). ESI-MS shows a mono-cation at $m/z = 1060.16$ (calcd 1060.16) with the correct isotope pattern. Crystallization (THF/pentane/-18 °C) gave a small number of crystals, for which a single-crystal X-ray diffraction study showed a $H_2B{=}NH_2$ unit bridging a $\{(Rh_2(L^{Ph})_2(\mu\text{-}H)\}$ unit (Supporting Information, Figure S21). However, insufficient material was obtained upon which to collect reliable NMR data. Complex **3** is unstable in solution at room temperature, decomposing after four hours to give a mixture in which $[Rh(L^{Ph})(THF)_2][BAr^F{}_4]$ **6** was present in approximately 30 % yield.[21] To put the structure and spectroscopic data on a firm footing, the equivalent reaction using the ^{i}Pr-substituted chelating phosphine gave complex **4**, $[Rh_2(L^{iPr})_2(\mu\text{-}H)(\mu\text{-}H_2B{=}NH_2)][BAr^F{}_4]$, and **5** (Scheme 2).

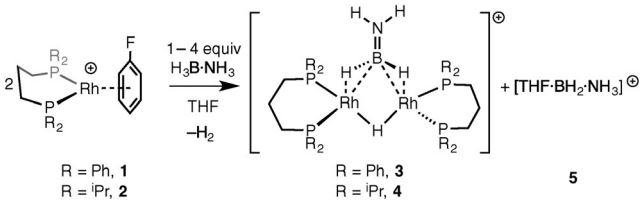

Scheme 2. Formation of amino-borane coordinated dimers **3** and **4**. $[BAr^F{}_4]^-$ anions are not shown.

This reaction was slower than that observed for L^{Ph}. Complex **4** can also be isolated in 78 % yield as orange crystalline material using an alternative route (see below, Scheme 5). In the absence of $H_3B{\cdot}NH_3$, complex **4** is stable for at least two days in $[D_8]$THF solution. However, when formed in situ **4** decomposes over 24 hrs into a mixture of products, one of which can be characterized as $[Rh_2(L^{iPr})_2(H)_2(\mu\text{-}H)_3][BAr^F{}_4]$.[22] The room temperature solution NMR data obtained for **4** are very similar to those for **3**: $\delta(^{11}B)$ 51.1; $\delta(^{31}P)$ 40.8, $J_{RhP} = 142$ Hz; $\delta(^1H)$ −8.64 (3 H, broad). Progressive cooling to 180 K splits the high field hydride resonance into two signals, in a 2:1 ratio; while two ^{31}P environments were also observed, suggesting a fluxional process at room temperature. An Eyring plot yields the activation data: $\Delta H^{\ddagger} = 31.1 \pm 1.3$ kJ mol^{-1}, $\Delta S^{\ddagger} = -27 \pm 1$ J K^{-1} mol^{-1}, $\Delta G(298\text{ K})^{\ddagger} = 39.2 \pm 1.6$ kJ mol^{-1}; where the negative entropy of activation suggests an intramolecular process (Supporting Information, Figures S2–3).

The solid-state structure of complex **4** is shown in Figure 1 A. A dimeric Rh_2 unit is accompanied by one $[BAr^F{}_4]^-$ anion, confirming that it is a mono-cation. Two $\{Rh(L^{iPr})\}^+$ fragments are bridged by a hydride and a $H_2B{=}NH_2$ unit. The B–N distance (1.377(6) Å) is consistent with a significant B–N π-interaction, and is similar to that measured in **A** (1.396(3) Å) and **B** (1.359(8) Å), as well as the bridging borylene complex **C** (1.399(3) Å; Scheme 3).[23] The Rh···B distances (2.070(5) and 2.055(5) Å) are similar to those found in the amino-borane complexes **A**, **B**, and $[Ir(PCy_3)_2(H)_2(H_2B{=}NMe_2)][BAr^F{}_4]$[24] (spanning 1.956(2) to 2.140(13) Å), but significantly shorter than those measured in the bridging thexylborohydride complex **D** (2.330(3) Å).[25] The hydrogen atoms were located but refined using a riding model. Within the limits of X-ray diffraction the B–H

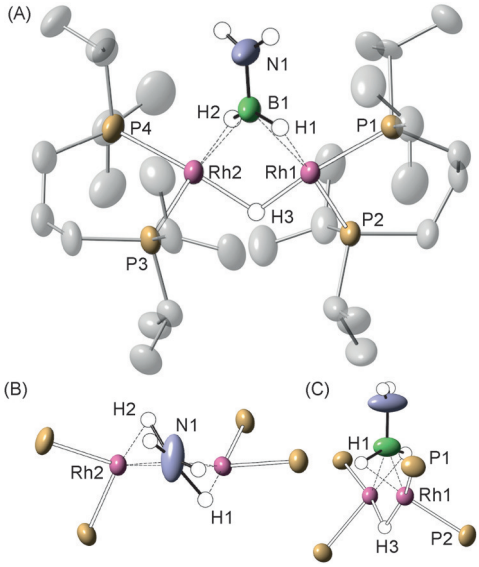

Figure 1. Solid-state structure of the cationic portion of complex **4**. Displacement ellipsoids are shown at the 50 % probability level. Selected bond distances (Å) and angles (°): Rh1···Rh2, 2.7874(4); Rh1–B1, 2.070(5); Rh2–B1, 2.055(5); B1–N1 1.377(6); P1–Rh1, 2.2550(10); P2–Rh1, 2.3063(10); Rh1–H1, 1.718; Rh2–H2, 1.723; ∡plane (N1B1H1H2)/plane (N1B1Rh1Rh2), 54.1; ∡plane (Rh1P1P2)/plane (Rh2P3P4), 100.2; ∡$(NH_2)/(BH_2)$ 24.3°.

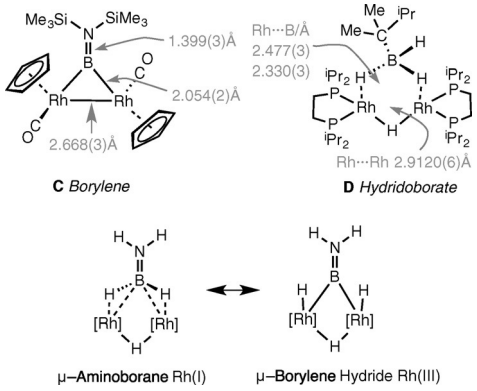

Scheme 3. Limiting valence bond descriptions for complex **4**, and examples of bridging hydridoborate and borylene complexes. [Rh] = $\{Rh(L^{iPr})\}$, charge not shown.

distances suggest lengthened, but unbroken bonds (for example, 1.360 Å). The NH_2 group is slightly twisted with respect to the BH_2 group (24.3°; Figure 1 B). The whole $H_2B{=}NH_2$ fragment lies 54.1° from the Rh-Rh vector so as to accommodate appropriate overlap between the B–H bonds and the two rhodium centers. These are best described as being two distorted square planes (for example, P1/P2/H3/H1) twisted with respect to one another by 102° (Figure 1 C). This motif, which is similar to that observed for **D**, is fully consistent with the low temperature NMR data, and are recreated well in the DFT calculated structure (Supporting Information, Figures S24–26). Each metal center in **4** is best described as Rh^I, with no M–M bond.[26] The end-on $\{Rh_2(\mu\text{-}H_2B{=}NH_2)\}$ binding mode contrasts with $H_2C{=}CH_2$ that bridges two metal centers symmetrically using both

carbon atoms, in either μ-η^2:η^2 or μ-η^1:η^1 bonding modes,[27,28] highlighting the differences between these isosteres.[29]

Surprisingly, the amino-borane in **4** is quite strongly bound. It is only slowly displaced by excess acetonitrile (7% in 50 min) to give a mixture of species, one of which is $[Rh(L^{iPr})(NCMe)_2][BAr^F_4]$.[22] No reaction occurs with toluene, which might be expected to form a $[Rh(L^{iPr})(\eta^6\text{-}C_6H_5Me)]^+$ complex if a monomeric $\{Rh(L^{iPr})\}^+$ fragment were accessible.[30] Addition of cyclohexene, shown to be a probe for free $H_2B{=}NH_2$,[2] gave no reaction. In contrast, H_2 rapidly reacts with **4** to form $[Rh_2(L^{iPr})_2(H)_2(\mu\text{-}H)_3][BAr^F_4]$.[22]

There are two limiting forms for the structure of **4** (and quasi-isostructural **3**): 1) a bridging amino-borane at two Rh^I centers, or 2) a bridging borylene dihydride (Rh^{III}), Scheme 3. The observed $\delta(^{11}B)$ chemical shift of 51 ppm is more consistent with the former as amino-boranes bound to one metal center show chemical shifts around 40–50 ppm,[12,13,24,31] while bridging borylenes[32] are generally observed between 90 and 100 ppm.[23,33]

To probe the bonding of the amino-borane ligand in **4**, DFT calculations were used as the basis for a Quantum Theory of Atoms in Molecules (QTAIM) analysis of the total electron density. The results are presented in Figure 2 A, along with selected bond critical point (BCP) metrics. Figure 2 B provides comparative BCP data for the bridging borylene complex **C**, the hydridoborate complex **D**, and $[(PPh_3)_2Rh(H)(\mu\text{-}H)(\mu\text{-}Cl)_2Rh(H)(PPh_3)_2]^+$, **E**, a well-defined Rh^{III} dimer with both terminal and bridging hydrides.[34] Average data are presented for all complexes where appropriate, although the discussion will focus on the bonding around a single rhodium center (Rh1).

In **4**, the {Rh1/B1/H1} moiety displays bond paths between all three centers, and these enclose a ring critical point (RCP). Thus, **4** has direct Rh1–B1 and Rh1–H1 bonding interactions, while the B1–H1 bond is also intact. Comparison with the Rh1–B1 interaction in **C** provides similar $\rho(r)$ and $H(r)$ values, but highlights a much reduced bond ellipticity (ε) of 0.08; this low value indicates dominant σ-bond character, whereas the value of 0.47 in **4** reflects the asymmetry introduced by the B1-H1 unit. In **D**, the absence of Rh-B BCPs confirms a lack of any direct Rh-B interaction, and this also reduces the average ellipticity of the Rh1–H1 and B1–H1 bonds. Also noticeable are the higher values of $p(r)$ and $H(r)$ for the terminal B1-H4 bond in **D** compared to the bridging B-H bonds in both that structure and, in particular, **4**, all of which is consistent with a weakening of the latter. For **E**, the Rh1-H1 BCP has larger values for $\rho(r)$ and $H(r)$ than the Rh1-H1 BCP in **4**, as well as a minimal ε value. These data indicate a terminal Rh–H σ-bond and stress the differences in bridging character of H1 and H2 in **4**. BCP data for the Rh1–H3–Rh2 bonds in **4**, **D**, and **E** are very similar, suggesting that this moiety varies little across these three systems.

Taken together, the QTAIM analyses suggest that **4** is best described as a μ-amino-borane Rh^I species; a μ-borylene hydride Rh^{III} formulism can certainly be ruled out in light of the intact B1–H1/B1–H2 bonds and the lack of Rh1–H1/Rh2–H2 terminal hydride character. The μ-amino-borane

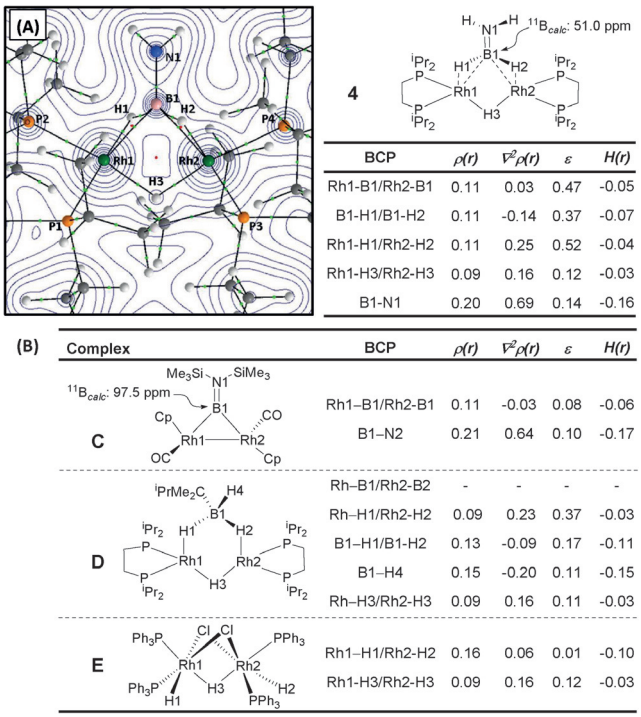

BCP	$\rho(r)$	$\nabla^2\rho(r)$	ε	$H(r)$
Rh1-B1/Rh2-B1	0.11	0.03	0.47	-0.05
B1-H1/B1-H2	0.11	-0.14	0.37	-0.07
Rh1-H1/Rh2-H2	0.11	0.25	0.52	-0.04
Rh1-H3/Rh2-H3	0.09	0.16	0.12	-0.03
B1-N1	0.20	0.69	0.14	-0.16

(B)

Complex	BCP	$\rho(r)$	$\nabla^2\rho(r)$	ε	$H(r)$
C ($^{11}B_{calc}$: 97.5 ppm)	Rh1–B1/Rh2-B1	0.11	-0.03	0.08	-0.06
	B1–N2	0.21	0.64	0.10	-0.17
D	Rh–B1/Rh2-B2	-	-	-	-
	Rh–H1/Rh2-H2	0.09	0.23	0.37	-0.03
	B1–H1/B1-H2	0.13	-0.09	0.17	-0.11
	B1–H4	0.15	-0.20	0.11	-0.15
	Rh–H3/Rh2-H3	0.09	0.16	0.11	-0.03
E	Rh1–H1/Rh2-H2	0.16	0.06	0.01	-0.10
	Rh1-H3/Rh2-H3	0.09	0.16	0.12	-0.03

Figure 2. A) Contour plot of the electron density of the central part of **4** presented in the {Rh1B1Rh2} plane with projected stationary points, bond paths, bond critical points (BCP; green), and ring critical points (RCP; red); the associated table shows selected BCP metrics (a.u.; average data for indicated bonds) and computed $\delta(^{11}B)$ chemical shifts. B) Calculated BCP metrics (a.u.; average data for indicated bonds) for comparator complexes **C** (including the computed ^{11}B chemical shift), **D** and **E** ($\rho(r)$ = electron density, $\nabla\rho(r)$ = Laplacian of electron density, ε = bond ellipticity, $H(r)$ = local energy density). All geometries are based on the crystallographically determined heavy atom positions with hydrogen atoms optimized with the BP86 functional. For a full summary of parameters see Figures S24–27 and associated Tables in the Supporting Information.

ligand in **4** interacts with the rhodium centers through stretched B–H bonds that engage in strong Rh-H and Rh-B interactions. Further support for this assertion comes from the computed $\delta(^{11}B)$ chemical shifts (Figure 2) and the Pipek–Mezey localized orbitals, where a strong bonding interaction spanning all three Rh1, B1, and H1 centers was identified (see Figure 3).

The mechanism of the room temperature fluxional process observed for **4** was also probed with DFT calculations and a single transition state was found to account for this process (Scheme 4). This is accessed by cleavage of one (blue) B-H bond to give a transition state structure featuring two Rh-H-Rh bridging hydrides; movement of the original (red) Rh-H-Rh hydride into a Rh-H-B bridging position then completes the exchange (**4′**). Repeating this process from **4′** exchanges a second B-H hydrogen (black) into the Rh-H-Rh bridging position (**4″**). The computed free energy of activation is 55.2 kJ mol^{-1}, somewhat higher than the experimental value (39.2 ± 1.6 kJ mol^{-1}) but still consistent with facile room temperature exchange.

Understanding how bimetallic species such as **3** and **4** are formed, and subsequently react, is important for delineating

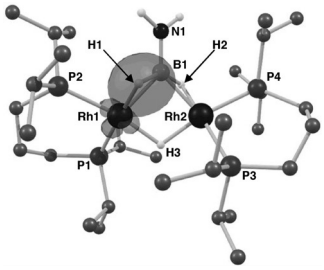

Figure 3. Pipek–Mezey localized orbital, highlighting the bonding interaction of the B1—H1 bond with center Rh1 (see Supporting Information, Figure S28, for details and related orbitals spanning the {Rh2B1H2} and {Rh1H3Rh2} moieties).

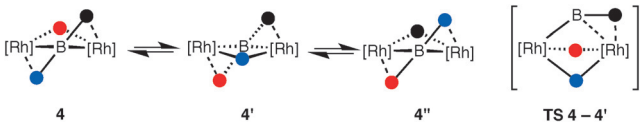

Scheme 4. Proposed fluxional process occurring in **4** (and **3**). Hydrogen atoms shown by filled circles. See Supporting Information for DFT calculated geometries and energies.

their role in amine-borane dehydrocoupling. The single equivalent of boronium $[THF{\cdot}BH_2{\cdot}NH_3][BAr^F{}_4]$ (**5**) formed indicates that a hydride abstraction route may be operating, as recently outlined by Conejero and co-workers for the dehydrocoupling of $H_3B{\cdot}NMe_2H$ by cationic $\{Pt\text{-}NHC\}^+$ catalysts,[17] as well as that occurring in cationic Ru/Ir-systems[35] or with $B(C_6F_5)_3$.[19] We reasoned that a similar process would yield **5** by B-H activation[16] and subsequent attack by THF (Scheme 5), alongside $\{Rh(L^R)H\}$

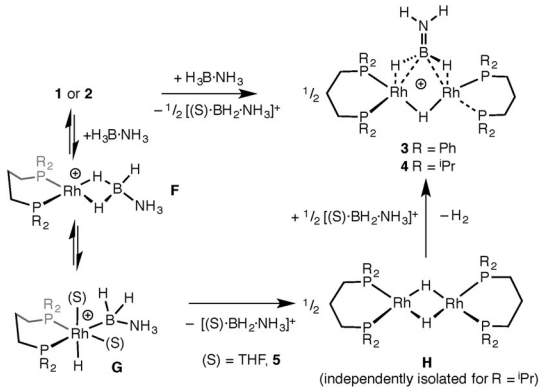

Scheme 5. Mechanism of formation of **3** and **4** by boronium protonation of neutral dimer **H**. (S) = THF or Et_2O. $[BAr^F{}_4]^-$ anions are not shown.

that would dimerize to give neutral $[Rh(L^R)H]_2$ (for example, complex **H**). Subsequent protonation[17] by boronium **5** and elimination of H_2 would give $H_2B{=}NH_2$ trapped on a rhodium dimer. To test this hypothesis, addition of **5** to the neutral dimer is required. $[Rh(L^{Ph})H]_2$ is unknown, and our attempts to prepare it have not been successful. $[Rh(L^{iPr})H]_2$ is a known complex, first prepared by Fryzuk in 1989,[36] and addition of one equivalent of the known boronium salt $[Et_2O{\cdot}BH_2{\cdot}NH_3][BAr^F{}_4]$[19] to $[Rh(L^{iPr})H]_2$ in Et_2O solvent, resulted in the immediate formation of **4** and gas evolution (H_2), which is consistent with the mechanism shown.

A dimeric species similar to **3** was also formed when one equivalent of $H_3B{\cdot}NMeH_2$ was added to **1** in THF solution. This was characterized by in situ NMR spectroscopy and ESI-MS as $[Rh_2(L^{Ph})_2(\mu\text{-}H)(\mu\text{-}H_2B{=}NMeH)][BAr^F{}_4]$ **8**: $\delta(^1H)$ −6.84; $\delta(^{31}P\{^1H\})$ 22.2, 21.5; $\delta(^{11}B)$ 50.6.[21] $[THF{\cdot}BH_2{\cdot}NMeH_2][BAr^F{}_4]$ was also formed ($\delta(^{11}B)$ 2.8 (t), $J_{HB} = 123$ Hz; lit. Et_2O adduct $\delta(^{11}B, CD_2Cl_2)$ 1.7 (t), $J_{HB} = 121$ Hz[9]). A more complex mixture of species was formed with $H_3B{\cdot}NMe_2H$, suggesting steric factors may be important in the formation of these aminoborane dimers, although a signal observed at $\delta(^{11}B)$ 52.7 suggests dimer formation. Complexes **3**, **4**, and **8** presumably form via a σ-complex $[Rh(L^R)(H_3B{\cdot}NRH_2)][BAr^F{}_4]$, R = H (**F** Scheme 5) or Me. In THF solution, using the L^{Ph} ligand, these σ-complexes were not observed as boronium formation and subsequent formation of **3** is fast. For L^{iPr}, an intermediate σ-complex could be observed on the way to **4**, $[Rh(L^{iPr})(H_3B{\cdot}NH_3)][BAr^F{}_4]$, presenting NMR data consistent with structure **F**.[21] Using $H_3B{\cdot}NMe_3$ (in which the N—H bonds are absent) $[Rh(L^{iPr})(H_3B{\cdot}NMe_3)][BAr^F{}_4]$ (**7**) was isolated and structurally characterized, confirming the in situ NMR studies (Supporting Information, Figure S23). The rapid reaction of $[Et_2O{\cdot}BH_2{\cdot}NH_3][BAr^F{}_4]$ with $[Rh(L^{iPr})H]_2$ to form **4** suggests protonation is not slow for this system; currently we cannot determine whether B—H activation or boronium formation is the rate limiting process, although it is likely that either could be promoted by excess amine-borane via N-H···H-B interactions.[37] Calculations on the $\{Pt\text{-}NHC\}^+/H_3B{\cdot}NMe_2H$ system suggest boronium formation is rate limiting.[17]

Complex **1** (0.5 mol%, THF, 3 hrs, open system) promoted the dehydrocoupling of $H_3B{\cdot}NH_3$ (1.2 equiv of H_2 evolved by gas burette; Supporting Information, Figures S4–S7) to form oligomeric species such as *B*-(cyclotriborazanyl)amine-borane (BCTB),[3,38] and insoluble polyaminoborane.[3] With more soluble $H_3B{\cdot}NMeH_2$, polymethylamino-borane was formed $[H_2BNMeH]_n$, which was isolated by precipitation from hexanes ($M_w = 30\,600$ g mol^{-1}, $Đ = 2.6$), alongside H_2 (1.1 equiv, gas burette). Consistent with the rapid formation of dimers such as **8** in THF, no induction period was observed (as measured by H_2 evolution) and similar TOF values were recorded (ca. 200 hr^{-1} for 1 equiv H_2), starting from monomeric **1** or in situ formed dimeric **8** (Scheme 6).[39] Changing the solvent to non-nucleophilic 1,2-$F_2C_6H_4$, and using **1** or in situ generated **8** as a catalyst, did not present an induction period and also revealed a faster TOF (for **8**, ca. 1000 hr^{-1} with 1 equiv of H_2 released).[40] Sub-catalytic in situ experiments in this solvent[21] show that dimer **8**, $[(BH_2)_2NMeH(\mu\text{-}H)]$ and boronium $[(NH_2Me)_2BH_2][BAr^F{}_4]$ are present;[41] the latter is suggested to arise from $NMeH_2$ formed from B—N bond cleavage in $H_3B{\cdot}NMeH_2$.[17] Thus, it is likely that similar active species are present in THF or 1,2-$F_2C_6H_4$. The lack of induction period is in direct contrast to xantphos-based rhodium catalysts, which show induction periods for $H_3B{\cdot}NMeH_2$ dehydrocoupling in C_6H_5F,[5,15] suggesting that a different kinetics regime or mechanism is in operation.

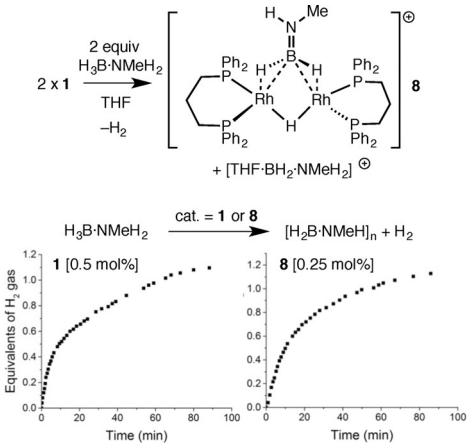

Scheme 6. H_2 evolution experiments using **1** or **8**, and $H_3B{\cdot}NMeH_2$ (0.5 mol% [Rh], 0.41 M amine-borane, THF, 298 K). $[BAr^F{}_4]^-$ anions are not shown.

Determination of the resting state in catalysis was hampered by the addition of excess amine-borane ($H_3B{\cdot}NH_3$ or $H_3B{\cdot}NMeH_2$) to the preformed dimeric species **3** or **4** in THF, resulting in a mixture of products that have been resistant to characterization. Turning to the pure and well-characterized dimer **4**, initial rate measurements in a closed system (4 mol% rhodium, THF) were more informative, and a first-order dependence for either $H_3B{\cdot}NH_3$ or $H_3B{\cdot}NMeH_2$, as well as catalyst **4**, were measured for the early pseudo zero-order phase of catalysis (Supporting Information, Figures S19 and 20). Such behavior is not consistent with a rapid dimer–monomer equilibrium for which an order of $[\mathbf{4}]^{1/2}$ would be expected,[22,36,42] a view supported by the stoichiometric reactions with acetonitrile or toluene (see above). Under these conditions complexes **2** or **4** do not promote full conversion of amine-borane (for **4**, 70% conversion of $H_3B{\cdot}NH_3$ after 10 hrs). Informed by the sub-catalytic experiments and H_2 addition studies, we propose that $[Rh_2(L^{iPr})_2(H)_2(\mu\text{-}H)_3][BAr^F{}_4]$[22] is formed during catalysis. Consistent with this hypothesis, isolated $[Rh_2(L^{iPr})_2(H)_2(\mu\text{-}H)_3][BAr^F{}_4]$ is a poorer catalyst for $H_3B{\cdot}NH_3$ dehydrocoupling in a sealed system (4 mol% [Rh], 30% conversion after 10 hrs) than both **2** and **4**. Interestingly, degassing the closed system restarted catalysis, indicating that inhibition by the H_2 formed during dehydrocoupling is partially reversible (Supporting Information, Figure S10). Co-promotion of dehydrocoupling by boronium is discounted, as these studies show that isolated **4** is an active pre-catalyst in its absence. Consistent with this statement, dehydrocoupling of $H_3B{\cdot}NH_3$ is not catalyzed by $[Et_2O{\cdot}BH_2{\cdot}NH_3][BAr^F{}_4]$ under the conditions used here (0.5 mol%, THF, 298 K, 3 hrs).[19] Overall, these observations do not let us discriminate between active catalysts derived from dimeric **4** (or **3**) or monomeric species that result from irreversible, but fast, consumption of **4** (or **3**), under the conditions of excess amine-borane.[43]

The ambiguity surrounding mono/bimetallic catalysis has parallels with xantphos-based amine-borane dehydropolymerization catalysts, where P-C activated phosphido-bridged species are formed that are also active catalysts, in contrast to the amino-borane-bridged dimers observed here.[15] Deconvoluting these systems under conditions of high amine-borane concentration is thus a significant challenge to address if precise control over the resulting polyamino-borane is to be achieved by metal/ligand design. Nevertheless, the observation of novel and unexpected bridging amino-borane complexes as the first-formed species, offers tantalizing clues as to the nature of the actual catalysts; and also suggests that boronium cations may play a more general role in amine-borane dehydrocoupling than generally appreciated.[17,19]

Acknowledgements

The EPSRC (A.S.W. and S.A.M., EP/M024210/1; N.A.B., DTP Studentship), the Rhodes Trust (A.K.), G. M. Adams (G. P. C. analysis).

Keywords: amino-borane · dehydrocoupling · DFT · catalytic mechanisms · rhodium dimers

How to cite: *Angew. Chem. Int. Ed.* **2016**, *55*, 6651–6656
Angew. Chem. **2016**, *128*, 6763–6768

[1] E. M. Leitao, T. Jurca, I. Manners, *Nat. Chem.* **2013**, *5*, 817; H. C. Johnson, T. N. Hooper, A. S. Weller, *Top. Organomet. Chem.* **2015**, *49*, 153; A. Staubitz, A. P. M. Robertson, M. E. Sloan, I. Manners, *Chem. Rev.* **2010**, *110*, 4023.
[2] V. Pons, R. T. Baker, N. K. Szymczak, D. J. Heldebrant, J. C. Linehan, M. H. Matus, D. J. Grant, D. A. Dixon, *Chem. Commun.* **2008**, 6597.
[3] A. Staubitz, M. E. Sloan, A. P. M. Robertson, A. Friedrich, S. Schneider, P. J. Gates, J. Schmedt auf der Günne, I. Manners, *J. Am. Chem. Soc.* **2010**, *132*, 13332.
[4] R. T. Baker, J. C. Gordon, C. W. Hamilton, N. J. Henson, P.-H. Lin, S. Maguire, M. Murugesu, B. L. Scott, N. C. Smythe, *J. Am. Chem. Soc.* **2012**, *134*, 5598; A. N. Marziale, A. Friedrich, I. Klopsch, M. Drees, V. R. Celinski, J. Schmedt auf der Günne, S. Schneider, *J. Am. Chem. Soc.* **2013**, *135*, 13342.
[5] H. C. Johnson, E. M. Leitao, G. R. Whittell, I. Manners, G. C. Lloyd-Jones, A. S. Weller, *J. Am. Chem. Soc.* **2014**, *136*, 9078.
[6] A. Glüer, M. Förster, V. R. Celinski, J. Schmedt auf der Günne, M. C. Holthausen, S. Schneider, *ACS Catal.* **2015**, *5*, 7214.
[7] J. F. Hartwig, *OrganoTransition Metal Chemistry*, University Science Books, Sausalito, **2010**.
[8] H. A. McGee, C. T. Kwon, *Inorg. Chem.* **1970**, *9*, 2458; J. S. Wang, R. A. Geanangel, *Inorg. Chim. Acta* **1988**, *148*, 185.
[9] O. J. Metters, A. M. Chapman, A. P. M. Robertson, C. H. Woodall, P. J. Gates, D. F. Wass, I. Manners, *Chem. Commun.* **2014**, *50*, 12146.
[10] H. C. Johnson, A. S. Weller, *J. Organomet. Chem.* **2012**, *721–722*, 17.
[11] G. J. Kubas, *Metal Dihydrogen and σ-bond complexes*, Kluwer, New York, **2001**; M. Shimoi, S. Nagai, M. Ichikawa, Y. Kawano, K. Katoh, M. Uruichi, H. Ogino, *J. Am. Chem. Soc.* **1999**, *121*, 11704.
[12] G. Alcaraz, L. Vendier, E. Clot, S. Sabo-Etienne, *Angew. Chem. Int. Ed.* **2010**, *49*, 918; *Angew. Chem.* **2010**, *122*, 930.
[13] M. C. MacInnis, R. McDonald, M. J. Ferguson, S. Tobisch, L. Turculet, *J. Am. Chem. Soc.* **2011**, *133*, 13622.
[14] R. Dallanegra, A. P. M. Robertson, A. B. Chaplin, I. Manners, A. S. Weller, *Chem. Commun.* **2011**, *47*, 3763.
[15] H. C. Johnson, A. S. Weller, *Angew. Chem. Int. Ed.* **2015**, *54*, 10173; *Angew. Chem.* **2015**, *127*, 10311.

[16] A. B. Chaplin, A. S. Weller, *Angew. Chem. Int. Ed.* **2010**, *49*, 581; *Angew. Chem.* **2010**, *122*, 591.
[17] M. Roselló-Merino, J. López-Serrano, S. Conejero, *J. Am. Chem. Soc.* **2013**, *135*, 10910.
[18] W. E. Piers, S. C. Bourke, K. D. Conroy, *Angew. Chem. Int. Ed.* **2005**, *44*, 5016; *Angew. Chem.* **2005**, *117*, 5142.
[19] F. H. Stephens, R. T. Baker, M. H. Matus, D. J. Grant, D. A. Dixon, *Angew. Chem. Int. Ed.* **2007**, *46*, 746; *Angew. Chem.* **2007**, *119*, 760.
[20] T. A. Shuttleworth, M. A. Huertos, I. Pernik, R. D. Young, A. S. Weller, *Dalton Trans.* **2013**, *42*, 12917.
[21] See the Supporting Information.
[22] A. Kumar, J. S. A. Ishibashi, T. N. Hooper, T. C. Mikulas, D. A. Dixon, S. Y. Liu, A. S. Weller, *Chem. Eur. J.* **2016**, *22*, 310.
[23] H. Braunschweig, M. Forster, T. Kupfer, F. Seeler, *Angew. Chem. Int. Ed.* **2008**, *47*, 5981; *Angew. Chem.* **2008**, *120*, 6070.
[24] G. Alcaraz, A. B. Chaplin, C. J. Stevens, E. Clot, L. Vendier, A. S. Weller, S. Sabo-Etienne, *Organometallics* **2010**, *29*, 5591.
[25] R. T. Baker, D. W. Ovenall, R. L. Harlow, S. A. Westcott, N. J. Taylor, T. B. Marder, *Organometallics* **1990**, *9*, 3028.
[26] J. C. Green, M. L. H. Green, G. Parkin, *Chem. Commun.* **2012**, *48*, 11481.
[27] W. H. Monillas, G. P. A. Yap, L. A. MacAdams, K. H. Theopold, *J. Am. Chem. Soc.* **2007**, *129*, 8090.
[28] O. P. Anderson, B. R. Bender, J. R. Norton, A. C. Larson, P. J. Vergamini, *Organometallics* **1991**, *10*, 3145.
[29] C. Y. Tang, A. L. Thompson, S. Aldridge, *Angew. Chem. Int. Ed.* **2010**, *49*, 921; *Angew. Chem.* **2010**, *122*, 933.
[30] S. D. Pike, I. Pernik, R. Theron, J. S. McIndoe, A. S. Weller, *J. Organomet. Chem.* **2015**, *784*, 75.
[31] G. Bénac-Lestrille, U. Helmstedt, L. Vendier, G. Alcaraz, E. Clot, S. Sabo-Etienne, *Inorg. Chem.* **2011**, *50*, 11039; C. Y. Tang, A. L. Thompson, S. Aldridge, *J. Am. Chem. Soc.* **2010**, *132*, 10578.
[32] H. Braunschweig, R. D. Dewhurst, V. H. Gessner, *Chem. Soc. Rev.* **2013**, *42*, 3197.
[33] H. Braunschweig, Q. Ye, A. Damme, K. Radacki, *Chem. Commun.* **2013**, *49*, 7593; H. Braunschweig, M. Colling, *Coord. Chem. Rev.* **2001**, *223*, 1.
[34] A. Rifat, N. J. Patmore, M. F. Mahon, A. S. Weller, *Organometallics* **2002**, *21*, 2856.
[35] R. Kumar, B. R. Jagirdar, *Inorg. Chem.* **2013**, *52*, 28; A. Rossin, M. Caporali, L. Gonsalvi, A. Guerri, A. Lledos, M. Peruzzini, F. Zanobini, *Eur. J. Inorg. Chem.* **2009**, *2009*, 3055.
[36] M. D. Fryzuk, W. E. Piers, F. W. Einstein, T. Jones, *Can. J. Chem.* **1989**, *67*, 883.
[37] A. Kumar, H. C. Johnson, T. N. Hooper, A. S. Weller, A. G. Algarra, S. A. Macgregor, *Chem. Sci.* **2014**, *5*, 2546; X. Chen, J.-C. Zhao, S. G. Shore, *Acc. Chem. Res.* **2013**, *46*, 2666; V. S. Nguyen, M. H. Matus, D. J. Grant, M. T. Nguyen, D. A. Dixon, *J. Phys. Chem. A* **2007**, *111*, 8844.
[38] H. A. Kalviri, F. Gärtner, E. Ye, I. Korobkov, R. T. Baker, *Chem. Sci.* **2015**, *6*, 618.
[39] An induction period for $H_3B{\cdot}NMe_2H$ dehydrocoupling using catalyst **1** in 1,2-$F_2C_6H_4$ solvent has been reported. See Ref. 14 and supporting materials. The lack of induction period observed using $H_3B{\cdot}NMeH_2$ may be a result of reduced steric effects that promote boronium formation. Related calculations using **1**/$H_3B{\cdot}NMe_2H$ have suggested that dimeric rhodium species are unlikely to be formed, in contrast to observations reported here: V. Butera, N. Russo, E. Sicilia, *ACS Catal.* **2014**, *4*, 1104.
[40] We were unable to fit the temporal evolution of H_2 to a simple kinetic profile in THF solvent. Interestingly, in 1,2-$F_2C_6H_4$ H_2 evolution appears to follow a zero-order profile, perhaps suggestive of saturation kinetics operating in this non-nucleophilic solvent.
[41] K. R. Graham, M. E. Bowden, T. Kemmitt, *Inorg. Chem.* **2011**, *50*, 932.
[42] Z. Lu, B. L. Conley, T. J. Williams, *Organometallics* **2012**, *31*, 6705.
[43] Heterobimetallic systems have been reported for the dehydrogenation of $H_3B{\cdot}NMe_2H$, see: T. Miyazaki, Y. Tanabe, M. Yuki, Y. Miyake, Y. Nishibayashi, *Organometallics* **2011**, *30*, 2394.

Received: January 26, 2016
Revised: March 22, 2016
Published online: April 21, 2016

